Chapter 1

The Large Hadron Collider

1.1 Introduction

The Large Hadron Collider (LHC by its initials in English) is the largest and most complex project built by mankind so far. It is part of the facilities of the European laboratory CERN, outside Geneva on the border between Switzerland and France and it is in a tunnel of 27 km of circumference excavated to a depth of 100 m.

The motivation for building the LHC arises from the need to answer fundamental questions in particle physics. Among these issues to be resolved is the mass: Does the Higgs boson exist? In the Standard Model of particle physics the Higgs plays an important role allowing the quarks, leptons and the W and Z bosons have mass. Moreover, there is strong, but indirect, evidence that nature has a symmetry called supersymmetry, which suggests that each particle has a superpartner. If nature is indeed supersymmetric the superpartners must exist and some can be detected at the LHC.

The LHC has been under development since the beginning of the 1980s. The CERN council approved the project in 1994. Initially it was proposed to build in two stages due to limited funds. But strong support for the LHC by CERN non-members of the council met and decided in 1996 that the LHC will be built in one step with beam energy of 7 TeV (Schmidt, 2003). In 2008, the accelerator was finished and on 10 September the same year the first particle beam successfully circled through the LHC (CERN Press Office, 2008).

1.2 Physical Principles of Functioning

The force on a particle with charge q and velocity $\mathbf{v}$ due to the presence of an electric field $\mathbf{E}$ and a magnetic field $\mathbf{B}$ is given by the Lorentz equation:

$$\mathbf{F} = (\mathbf{E} + \mathbf{v} \times \mathbf{B}). \tag{1.1}$$

The energy increase is obtained from the electric field and magnetic field is used to change the trajectory of charged particles. The energy gain of a particle by an electric field is given by:

$$\Delta E = \int_{s_1}^{s_2} \mathbf{F} \cdot d\mathbf{s}. = \int_{s_1}^{s_2} q\mathbf{E} \cdot d\mathbf{s} = qV. \tag{1.1}$$

For acceleration to 7 TeV/c, it requires a voltage of 7 TeV. Since it is not possible to accelerate particles to such energy using a constant potential, radiofrequency (RF) is used. In a radio frequency cavity, time-varying electric field accelerates to the charged particles what must enter into cavity with the correct phase. If a particle comes later in incorrect phase it would be slowed. As a result of the use of an RF system we have discrete beams formed by bunches of particles, it is not possible to accelerate a continuous beam (Schmidt, 2003). Since the LHC is a circular accelerator, particles will circulate many times through RF cavities where they will be accelerated with each lap. Dipole magnets are used to keep the particles during acceleration in a (roughly) circular orbit. The LHC RF systems operate at 400 MHz (Boussard and Linnecar, 1999).

The deflection of charged particles in a magnetic field is also determined by the Lorentz force:

$$\mathbf{F} = m\mathbf{a} = q(\mathbf{v} \times \mathbf{B}). \tag{1.2}$$

Assuming that the particle moves in a circle with radius ρ in a uniform magnetic field perpendicular to the velocity, the Lorentz force equals the centrifugal force:

$$qvB = m\frac{v^2}{\rho}. \tag{1.3}$$

The radius of the accelerator is determined by the energy of the particle and magnetic field strength:

$$\rho = \frac{E}{cqB}. \tag{1.4}$$

The bending radius of the magnets is determined by the LHC tunnel. At injection energy of 450 GeV the magnetic field is 0.54 T. During acceleration, the field in the dipole magnets is increased to 8.33 T for getting a maximum energy of 7 TeV. Such a field is obtained with superconducting magnets (Rossi, 2004).

1.3 Synchrotron Radiation

Electrons and protons moving in a circular accelerator emit synchrotron radiation due to longitudinal acceleration by electric fields and transversal acceleration when the particles are deflected. The power emitted by the longitudinal acceleration is very small and can be neglected. The power emitted by a particle that is deflected is given by (Wilson, 2001):

$$P = \frac{e^2 c}{6\pi\varepsilon_0 (m_0 c^2)^4} \frac{E^4}{\rho^2}. \tag{1.5}$$

A proton in the LHC at 7 TeV lost 8.1×10^3 eV per lap. The total power loss due to synchrotron radiation for the LHC-type beam, with 3×10^{14} protons, is 2700 W. This is dissipated in a cryogenic system. This system keeps the superconducting magnets at a temperature of 1.9 K using helium in superfluid state.

1.4 Principal Characteristics

The LHC is divided into eight octants containing to eight arcs sections, eight straight sections, experiments and operating systems of the machine (see Figure 2.1). Two beams of particles with opposite rotation, circulate in separated tubes installed in the twin opening (Gupta, 1998) of the magnets and they are crossed in four interaction points. The beams collide at a small angle in the center of the experimental detectors: ATLAS, ALICE, CMS and LHCb.

The transport of particles through the arches requires both dipole and quadrupole magnets for focusing. Quadrupole magnets focus the particles in a manner similar to lenses used in optics. The focusing is done at two levels: the horizontal plane (parallel plane to the circumference of the accelerator) and the vertical plane (plane perpendicular to the above). For focusing the beams in both planes, a series of focusing-defocusing quadrupole magnets with drift space between them is required, this structure is known by the name of FODO (Chao y Tigner, 1998).

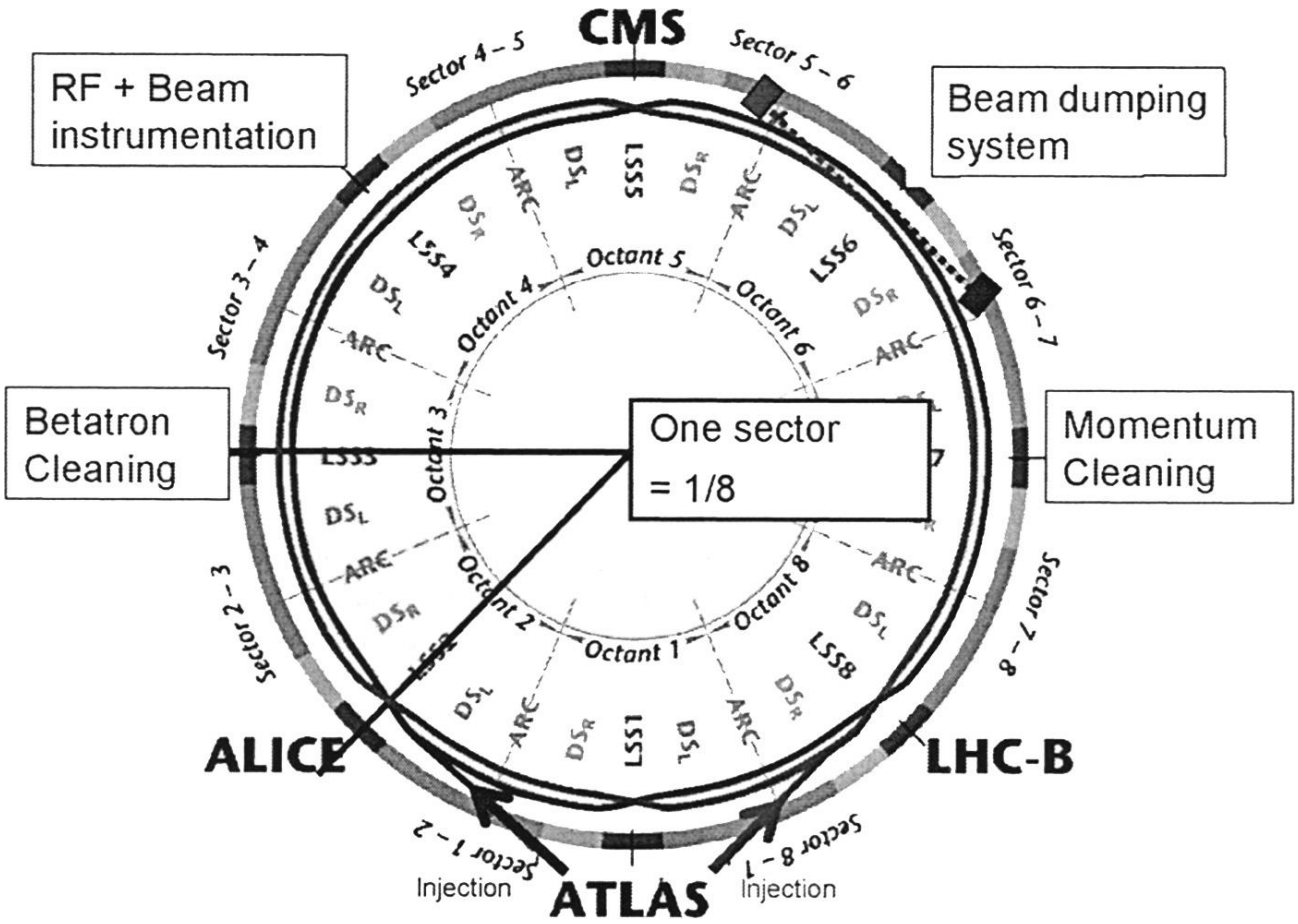

Figure 1.1 Schematic layout of the Large Hadrons Collider.

Each of the LHC arcs consists of 23 regular cells. Each cell consists of six dipole magnets to bend the particle trajectory and two quadrupole magnets with opposite polarities, for focusing on both levels (see Figure 1.2). The accelerator's network is determined by the position of the dipole and quadrupole magnets along the same. The network along with the intensity of the magnets determines the optical of the beam.

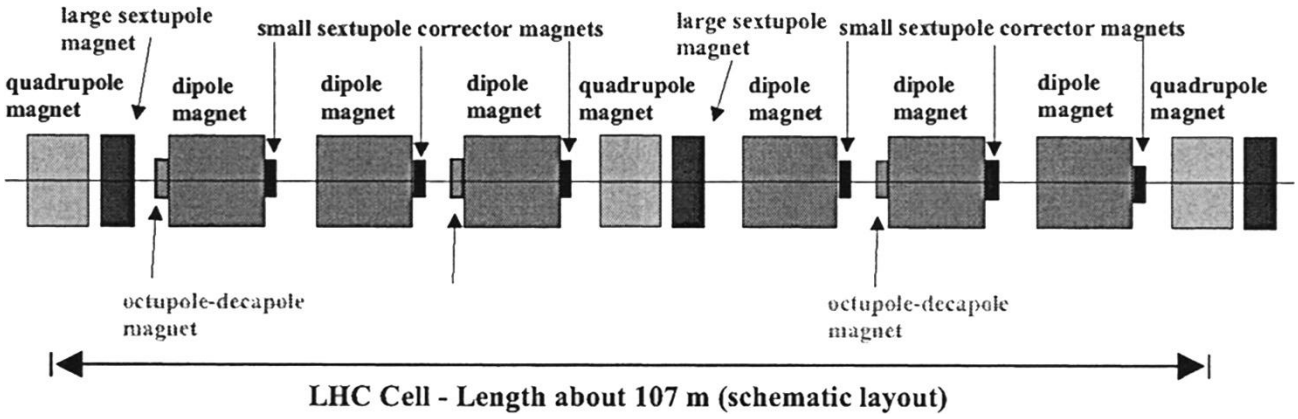

Figure 1.2 Schematic layout of a LHC cell with dipoles, quadrupoles and correction magnets.

With an appropriate coordinate transformation, can be shown that using only dipole and quadrupole magnets, the trajectories of the particles can be stable. In this coordinate system the motion of particles is described as a harmonic oscillation due to the linear driving force of a quadrupole magnet (betatron oscillation). An important parameter of circular accelerators is the betatron tune, i.e. the number of oscillations of a particle in one turn, for each plane. The transverse size of the beam along the accelerator is given by $\sigma = \sqrt{\varepsilon\beta}$. The emittance ε_x (and ε_y for the vertical plane) is the phase space area, $\beta_x(s)$ y $\beta_y(s)$ are the so-called beta functions. For each plane, the beam size is proportional to the square root of the beta function. The functions depend on the beam optical and vary along the accelerator.

1.4.1 Luminosity at the LHC

When two bunches cross in the center of a detector, only a small fraction of the particles collide to produce the desired events. The ration of particles created in collisions is given of cross section and brightness: $N = \sigma_{cross} L$. For taking advantage of the LHC's energy range, luminosity of the order of 10^{34} $cm^{-2}s^{-1}$ is required. The luminosity L is increased with the number of protons in each bunch, and decreases with the size of the beam according to the relationship (Bhat, 2009):

$$L = \frac{N_b^2 f_{rev} n_b}{4\pi\sigma_{trans}^{*2}} F \cong \frac{N_{b\,rev}^2 n_b}{4\pi\sigma_{trans}^{*2}} \times \frac{1}{\sqrt{1+\left[\frac{\theta_c \sigma_z}{2\sigma_{trans}^*}\right]^2}} \tag{1.6}$$

where n_b, f_{rev}, N, θ_c y F are the numbers of bunches, the revolution frequency, number of protons per bunch, the crossing angle of two beams at the interaction point and a geometric correction factor, respectively. The amount $\theta_c \sigma_z / 2\sigma_{trans}^*$ is known as the angle of Piwinski. For maximizing the luminosity with a fixed number of particles per bunch we usually need to choose the crossing angle and the length of the bunch as small as possible, i.e. minimize the angle of Piwinski. In order to achieve the design LHC luminosity, each particle beam is composed of 2808 bunches.

1.5 Proposed Extensions for LHC's High Luminosity

There are three main reasons for making improved extensions of the LHC: the lifetime of the magnets in the interaction regions, which is eight years, the time needed to halve the statistical error of experimental measurements and extending the potential of the LHC at higher luminosities, which will increase the range of discovery of new particles (Ruggiero and Zimmermann, 2004).

The proposed extensions will be discussed briefly in the following sections.

1.5.1 Early Separation Scheme.

Early separation (ES) scheme's principle requires the installation of moderate dipole field magnets as close as possible to the interaction point (Koutchouk and Zimmermann, 2009). This scenario involves the installation of new hardware inside ATLAS and CMS detectors, as well as the use of crab cavities which can reduce the Piwinski angle to zero and thereby increase the luminosity (Scandale and Zimmermann, 2007).

1.5.2 Large Piwinski Angle Scheme

In the large Piwinski angle (LPA) scheme the spacing between bunches is increased twice, 50 ns; longer, more intense and longitudinal-plane bunches are collided with a large Piwinski angle: $\phi \equiv \theta_c \sigma_z / (2\sigma^*) \approx 2$, the beta function at the interaction point is increased by a factor of two, $\beta^* \approx 0.25$ m. This scheme permits increase the intensity of bunch, N_b, in (1.7) and therefore the luminosity remains constant. The advantages of the LPA scheme are the absence of accelerating elements within the detector, crab cavities are not required (Scandale and Zimmermann, 2007).

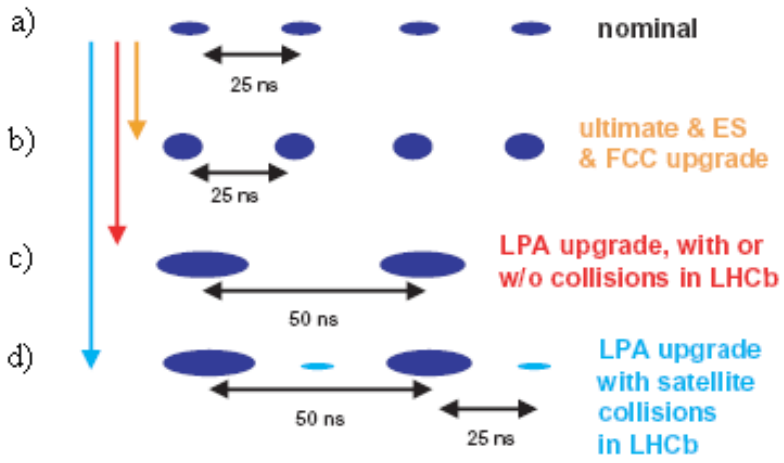

Figure 1.3 Structure of the bunches for the schemes: a) nominal and maximum LHC performance, b) ES/FCC, c) LPA and d) LPA with satellite bunches.

1.5.3 Compatibility Scheme with the LHCb Experiment

An upgrade to the LHCb experiment is planned in order to exploit luminosity of around 2×10^{33} $cm^{-2}s^{-1}$ or 2% of the luminosity delivered to the ATLAS and CMS experiments. The LHCb detector is special because of its asymmetric position in the circumference of the LHC. In the LPA scheme, discussed above, we can add satellite bunches between the main bunches as illustrated in Figure 1.3d. These satellites can collide in the LHCb with the main bunches of another particle beam at time intervals of 25 ns.

Chapter 2

Electron Cloud in the LHC

2.1 Origin of the Electron Cloud

The LHC is an accelerator where synchrotron radiation becomes noticeable. At energy of 7 TeV, the relativistic factor γ is comparable to the beams of electrons or positrons from many sources of light. The critical energy of synchrotron radiation is about 44 eV, which is close to the maximum rate of photoemission energy (i.e. the number of photoelectrons per incident photon) for many materials. Therefore, the electron cloud emerges from a process of multiple impacts of the electrons within the vacuum chamber. At the LHC, the electrons are produced when residual gas molecules are ionized by protons and also when the synchrotron radiation beam strikes the beam screen (a shield of stainless steel covered with copper inserted in the arch of the vacuum chamber, which absorbs photons of synchrotron radiation). Such electrons have typical energies of the order of eV and are still within the beam screen when the next bunch passes, the field of the bunch is sufficient to accelerate these electrons to energies of about 100 – 1000 eV. After the bunch passage, the accelerated electrons reach the beam pipe walls, before the next bunch arrives, they hit the wall, producing one or more secondary electrons (Diaczenko et al., 2005) Figure 2.1 presents an outline of the process that leads to the electron cloud.

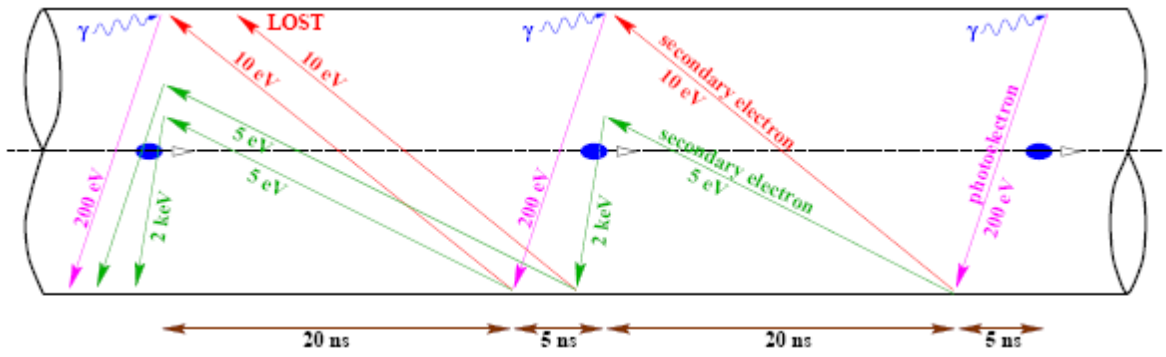

Figure 2.1 Schematic layout of the electron cloud build-up in the LHC.

2.2 Electron Cloud Effects

The electron cloud can cause instabilities on the proton beam, because they are attracted to the cloud of negatively charged electrons, causing the beam increases in size or can cause the beam to swing out of control (Vance, 2006).

On the other hand, can also cause increased pressure, by several orders of magnitude, due to electron-stimulated desorption (Jimenez et al., 2002).

Finally, a primary concern for the LHC is the additional heat load due to the electron cloud that is deposited on the beam screen. Only a limited cooling capacity is available for additional heat load, if it is exceeded the superconducting magnets could lose their superconducting state (Zimmermann and Benedetto, 2004). This last point is to be studied in this thesis work because it can limit the optimum performance of the LHC.

2.3 Measures for the Suppression of the Electron Cloud

The design of the LHC has taken several steps to counter the effects of the electron cloud. For example, many sections of the vacuum chamber in the hot sections of the LHC have been covered by a getter material, TiZrV (Benvenuti, 2001) with this material have achieved low rates of secondary electron emission. In cold sections of the LHC coatings have been implemented using surfaces with a sawtooth pattern. This pattern has an impact, locally, on photons emitted by synchrotron radiation resulting in a reduction in the reflectivity and a lower rate of photoemission (Baglin, 1998). Moreover, the heat load on the beam screen and the pressure in the vacuum chamber may be confined to acceptable limits by reducing the number of bunches or the intensity of they (Caspers et al., 2009).

2.4 Simulation of the Electron Cloud Built-up

Proper understanding of the electron cloud effects requires tools capable of simulating the growth of the cloud. One of such tools is the ECLOUD code, created by Dr. Frank Zimmermann in 1997, which has been refined through support of researchers: O. Bruning, X.-L. Zhang, G. Rumolo,

D. Schulte and G. Belloti. At the same time, the code has been improved with the comparison of code predictions with experimental date obtained from the SPS using LHC-like type beams (Arduini et al., 2004).

2.4.1 Physical Principles of the ECLOUD code

The number of photons emitted by a charged particle per radian is (Sands, 1970):

$$N_\gamma = \frac{5}{2\sqrt{3}}\alpha\gamma \tag{2.1}$$

where α is the fine structure constant and γ is the relativistic Lorentz factor. In the LHC, at energy of 7 TeV, this amount is about $3.7\text{x}10^{10}$ photons per bunch. The typical rate of photoemission at energies of 10-100 eV is 0.1 (Kouptsidis and Mathewson, 1976). ECLOUD code assumes that on average a photon that hits the surface of the beam tube is reflected or converted into a photoelectron, so that eventually the total number of photoelectrons is approximately equal to the number of radiated photons. Under this assumption, each photon is reflected up to 10 times before it makes a photoelectron, and the impact location on the surface is considered aleatory. For this reason the simulation launch photoelectrons uniformly distributed around the beam pipe opening (which is idealized with an ellipse), with an initial uniform energy distribution between 0 and 10 eV.

The photoelectrons emitted from the surface are accelerated by the field of the beam. A photoelectron generated by synchrotron radiation emitted from the front of the bunch takes a maximum transverse moment given by

$$\Delta p_{el} \approx \frac{2N_b r_{el} c m_{el}}{r_{pipe}}, \tag{2.2}$$

where r_e denotes the classical electron radius, c is the speed of light, r_{pipe} is the beam pipe radius, m_{el} is the electron mass y p_{el} is the electron's momentum. For the LHC, it corresponds to an energy of

$$\Delta E_{el} \approx \frac{1}{2} m_{el} c^2 \left(\frac{v}{c}\right)^2 \approx 200 \text{ eV}, \tag{2.3}$$

and flight time from wall to wall about 1.5 m/c. The photoelectrons created by radiation from the back of the bunch only see a fraction of the maximum energy of 200 eV, and the flight time from wall to wall is bigger. Since the spacing between bunches is 7.5 m, many of the primary photoelectrons hit the beam pipe surface before the next bunch arrives. When and electron, with an energy of 200 eV, incidents on the surface secondary electrons are emitted. The speed of these secondary electrons is a factor of 5 – 10 lower than that of the primary electrons, then they are accelerated, along with new photoelectrons generated when the next bunch passes.

A large part of the LHC circumference is dominated by strong dipole field magnets where the electron motion is restricted to the vertical direction. However, the straight sections constitute 20% of the LHC circumference and electron dynamics is different so a different algorithm is used for simulation. In contrast, in a straight section, the electron feels a force both horizontal and vertical with the bunch passage (Zimmermann, 1997).

It is considered that each bunch has a longitudinal and uniform charge distribution. It is assumed that the bunches flow through the center of the beam pipe. The photoelectrons generated per bunch are represented by a set of variable number of macro particles. Typically, the code generates 1000 macro-photoelectrons for each bunch. The charge of the macro-particles is chosen in such way that is equal to the real one.

Each bunch is divided into 5 parts. After each new piece, photoelectrons are released. The space between each bunch is divided into a number of steps typically 7 to 12. At each step the motion of all macro particles is calculated.

When an electron beam strikes the beam screen, throw one or more secondary electrons at the point of impact. The field generated by the electron cloud is also included in the simulation. An outline of the simulation process described above is shown in Figure 2.2.

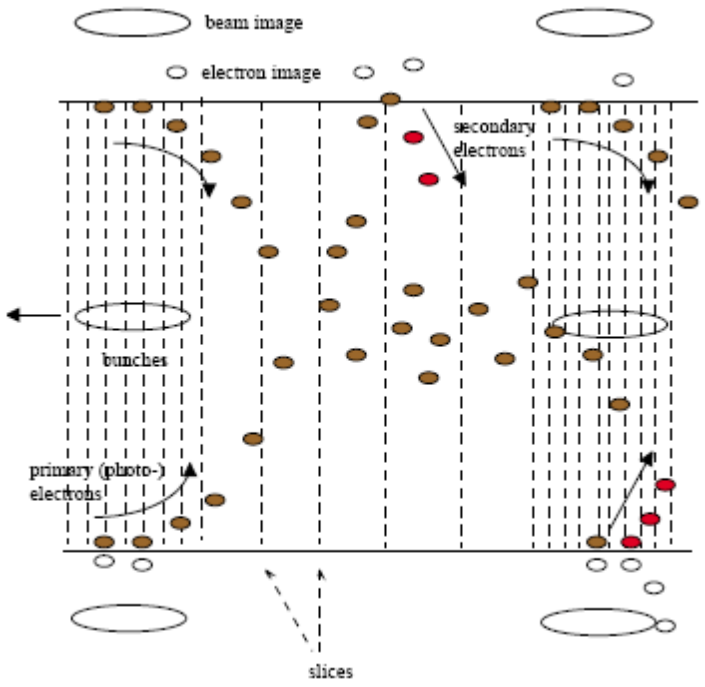

Figure 2.2 Schematic layout of the simulation process of the electron cloud build-up.

2.4.2 Secondary Electron Emission

The simulation results depend on heavily on the model assumed for the secondary emission ratio (SEY). ECLOUD takes into account two different contributions to the secondary emission: the true secondary electrons and primary electrons that are reflected. Thus, the total secondary emission yield is expressed as the sum of these two components:

$$\delta_{tot}(E_p,\theta) = \delta_{true}(E_p,\theta) + \delta_{el}(E_p,\theta). \tag{2.4}$$

The equation 2.4 is a function of primary electron energy, E_p , and the impact angle with respect to the normal surface, θ. The true emission rate as a function of impact energy E_p is given by the Furman formula (Furman and Lambertson, 1997):

$$\delta_{true}(E_p) = \delta_{\max}(\theta)\frac{s\dfrac{E_p}{E_{\max}}}{s-1+\left(\dfrac{E_p}{E_{\max}}\right)^s}, \tag{2.5}$$

where $s \approx 1.35$ and the two adjustable parameters $\delta_{\max}$ y $E_{\max}$ describing the maximum rate and the energy at what it is achieved. The dependence on the angle θ is inferred from experimental measurements. For $E_{\max}$ we have (Furman and Lambertson, 1997):

$$E_{\max}(\theta) \approx E_{\max}^{0}[1+0.7(1-\cos\theta)] \tag{2.6}$$

and $\delta_{\max}$ is expressed as (Kirby and King, 2000):

$$\delta_{\max}(\theta) \approx \delta_{\max}^{0} \exp[0.5(1-\cos\theta)], \tag{2.7}$$

where quantities with superscript 0 are referring to normal incidence.

The reflected component of the secondary electrons is significant at low impact energies. Based on experimental data, the elastic electronic reflectivity is given by (Cimino et al., 2003):

$$\delta_{el} = \frac{\sqrt{E_p + E_0} - \sqrt{E_p}^{\,2}}{\sqrt{E_p + E_0} + \sqrt{E_p}^{\,2}}. \tag{2.8}$$

The adjustable parameter E_0 has a value of 150 eV, which was derived from measurements in the work of Cimino et al., 2003.

2.4.3 Boundary Conditions

The fields produced by the beam and the electron cloud depend on the shape of the beam pipe and the image charges and image currents produced in the inner surface. The LHC beam pipe has a round cross-section with flat parts at the top and bottom, as shown in Figure 2.3a.

As shown in Figure 3.3b, the real geometry of the beam pipe has been replaced by an ellipse, which also forms the boundary for the calculation.

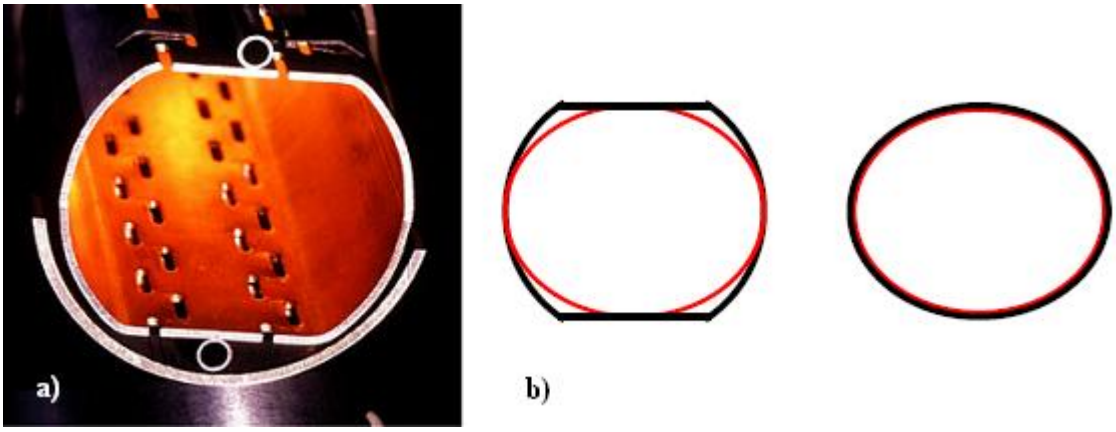

Figure 3.3 a) Cross section of beam pipe, showing the round, but flat at the ends, shape (image courtesy of CERN), b) the beam pipe is modeled by using an elliptical boundary.

2.4.4 Tracking of the Electrons

Different routines are used to track the cloud of electrons depending on the magnetic field in the beam pipe. In the absence of magnetic field, the tracking is easy, while for the case with field is not so simple because the electrons are strongly affected by it. To optimize the performance of the tracking program of electrons in magnetic fields are considered two types: dipole and quadrupole magnetic fields.

Tracking in Dipole Magnetic Fields:

For this case, the path of the electrons is determined analytically as the magnetic field has only a vertical component and the electron has a helical motion around the field lines. For tracking we use an integrator algorithm of differential equations.

Tracking in Quadrupole Magnetic Fields:

The simulation of a quadrupole magnetic field is the event that consumes more computation time. Instead of using the algorithm that solves the differential equations we have been used a faster algorithm based on the Bulirsh-Stoer method (Weisstein, 2009). The routine used adaptive step sizes. Each time interval is passed several times, with an increase in the number of steps. At each steps, it is assumed that the field is locally homogeneous, such that the particle moves in a helix. The results of the different passages of the same time interval are extrapolated to an infinite number of

steps which gives the final results. As we mentioned this routine is similar to Bulirsh-Stoer algorithm, but takes advantage of the analytic solution for a homogeneous field (Schulte and Zimmermann, 2007).

Chapter 3

Methodology

3.1 Introduction

For this thesis was used the ECLOUD program version 3.2 to simulate the electron cloud build-up and the heat load in the LHC. The program gives as results the heat load per LHC arc section with dipole and quadrupole magnets and per drift section. Later, we took the average of these sections, to have the total heat load.

3.2 Characteristics of the Simulations

We made eight sets of simulations whose characteristics are listed in Table 3.1. The physical parameters that were varied are: the spacing between bunches, the bunch profile, the number of protons per bunch, the secondary emission yield and the bunch length.

Set	Secondary emission yield (SEY)	Bunch spacing (ns)	Number of particles per bunch (N_b)	Bunch profile	Bunch length (cm)
A	1.1 – 1.7	25	$2 \times 10^{10} – 18 \times 10^{10}$	Gaussian	7.55
B	1.1 – 1.7	50	$2 \times 10^{10} – 18 \times 10^{10}$	Gaussian	
C	1.1 – 1.7	50	$20 \times 10^{10} – 60 \times 10^{10}$	Flat	
D	1.1 – 1.7	50	$1 \times 10^{10} – 50 \times 10^{10}$	Flat	11.8
E	1.1, 1.3, 1.5, 1.7	50	$1 \times 10^{11} – 5 \times 10^{11}$	Flat	41
F	1.1, 1.3, 1.5, 1.7	50	$1 \times 10^{11} – 5 \times 10^{11}$	Flat	
G	1.1, 1.3, 1.5, 1.7	5 – 50	$6 \times 10^{10} – 2.3 \times 10^{11}$	Flat	
H	1.1, 1.3, 1.5, 1.7	5 - 50	$6 \times 10^{10} – 2.3 \times 10^{11}$	Gaussian	7.55

Table 3.1 Summary of the sets of simulations.

The set A corresponds to simulations made using LHC nominal values, the set B also uses the nominal values but the only difference is the bunch spacing of 50 ns instead of design spacing of 25 ns, this set is an alternative scheme using LHC design values. The set C is an improved extension of the LHC where the number of particles per bunch (N_b) is increased to higher values, so this corresponds to a high luminosity scenario. The set D is another proposed extension of the LHC high luminosity where we use, instead of the nominal Gaussian bunch profile, a flat bunch profile. The set E is a special case where a flat bunch profile is considered. We have a main bunch every 50 ns but there is a satellite bunch between two main bunches. This is a proposed extension of compatibility with the LHCb experiment in order to have collisions in LHCb, ATLAS and CMS at the same time. We can do that if we take advantage that LHCb requires less luminosity than the other two. The set F has the same characteristics as set E, but with the difference of not having satellite bunches, this set served to compare the heat load produced by the satellites.

Finally, the sets G and H are a study of the heat load in function of the bunch spacing for a flat and Gaussian bunch profile, respectively. These two sets of simulations were performed to explore the dependence of the heat load with the bunch spacing.

Chapter 4

Results

4.1 Results of Simulations for the LHC Nominal Operation

According to the methodology explained in the previous chapter, we presented the plots of the average heat load for the simulation sets A, B and D.

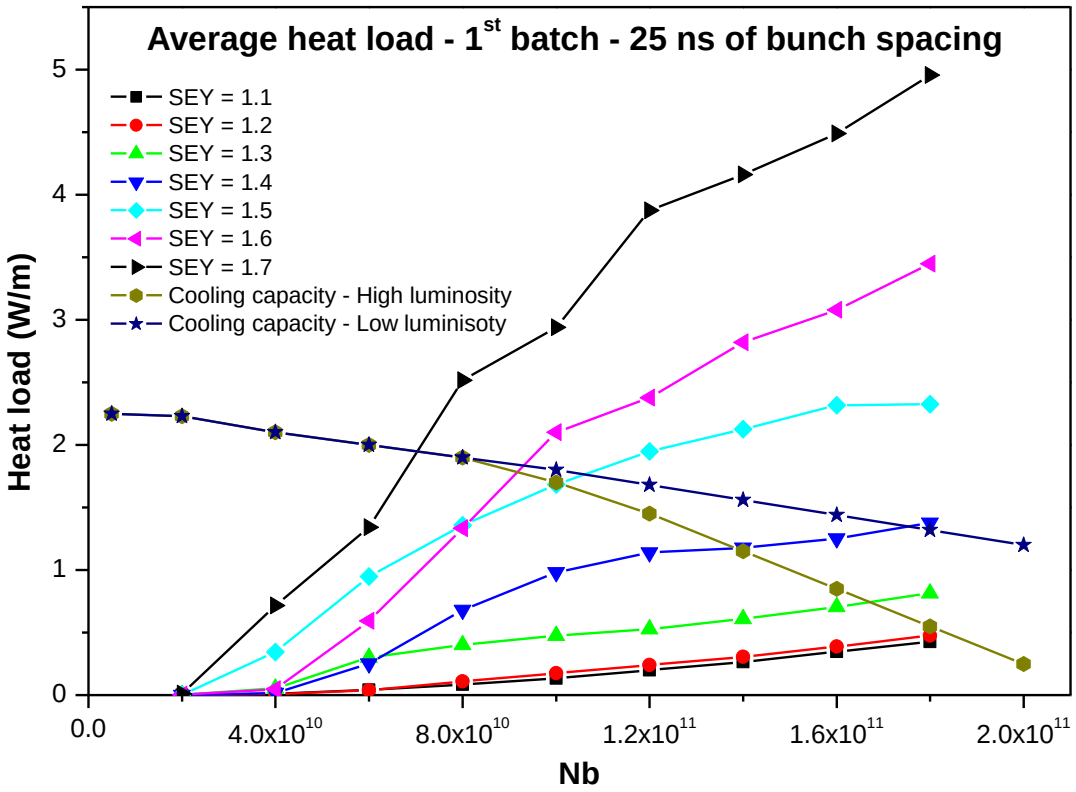

Figure 4.1 Average heat load for the simulation set A, 1st batch.

As shown in Figure 4.1 the heat load depends on the secondary emission yield (SEY) and the number of particles per bunch (N_b). For some values of SEY and N_b the average is below of the cooling capacity, which is acceptable, but for higher values the average is well above the cooling capacity.

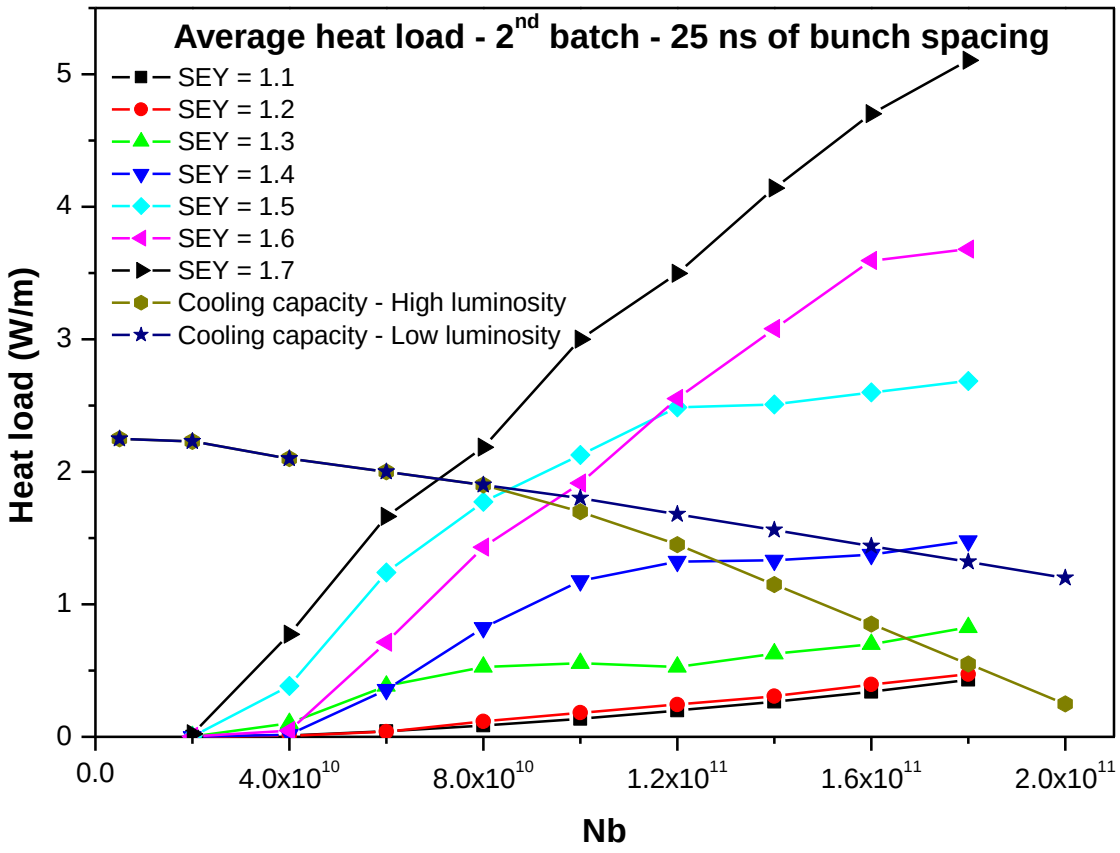

Figure 4.2 Average heat load for the simulation set A, 2nd batch.

In Figure 4.2, we can see the average heat load for the second batch corresponding to the simulation set A. As we can see, there is a noticeable difference between the heat load of the first batch and the second one.

Data collected for the first batch of the simulation set B are shown in Figure 4.3. As we can see the average heat load is well below the cooling capacity for any SEY value and N_b. In fact, the maximum observed value of the heat load is 0.25 W/m for a SEY = 1.7 and N_b = 1.8 x 10^{11} which is below the 0.55 W/m of the cooling capacity in that point. Figure 5.4 corresponds to the average heat load for the second batch. Again, there is no difference between the first and second batch.

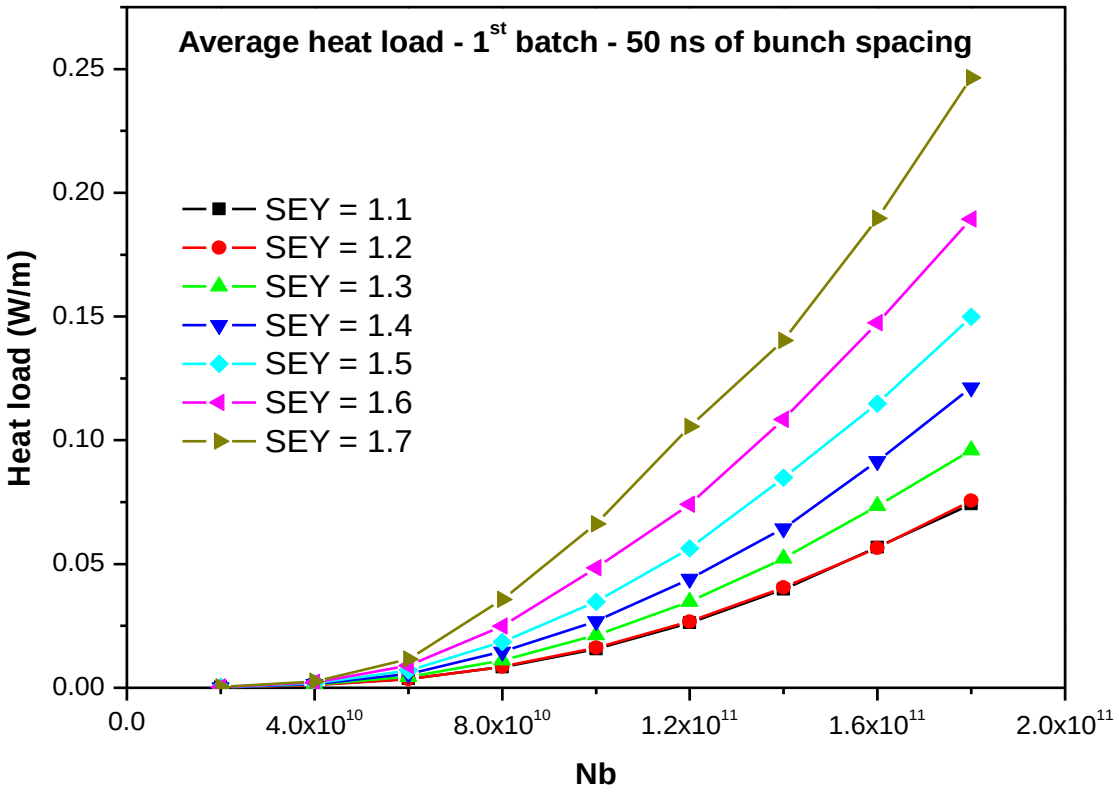

Figure 4.3 Average heat load for the simulation set B, 1st batch.

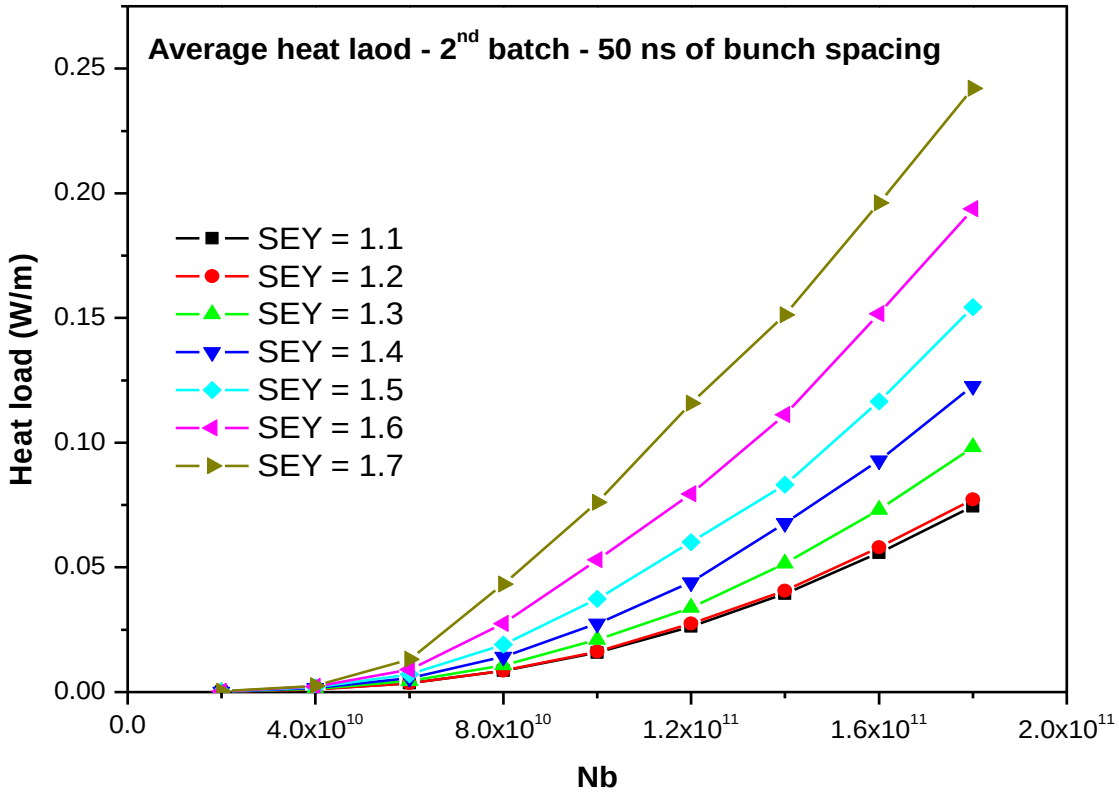

Figure 4.4 Average heat load for the simulation set B, 2nd batch.

4.2 Results of Simulations for the Proposed Extensions of the LHC

4.2.1 ES/FCC Scheme

In Figure 4.5, we see that for the high-luminosity proposed extension: ES/FCC scheme, it has an average heat load for some cases, above from cooling capacities.

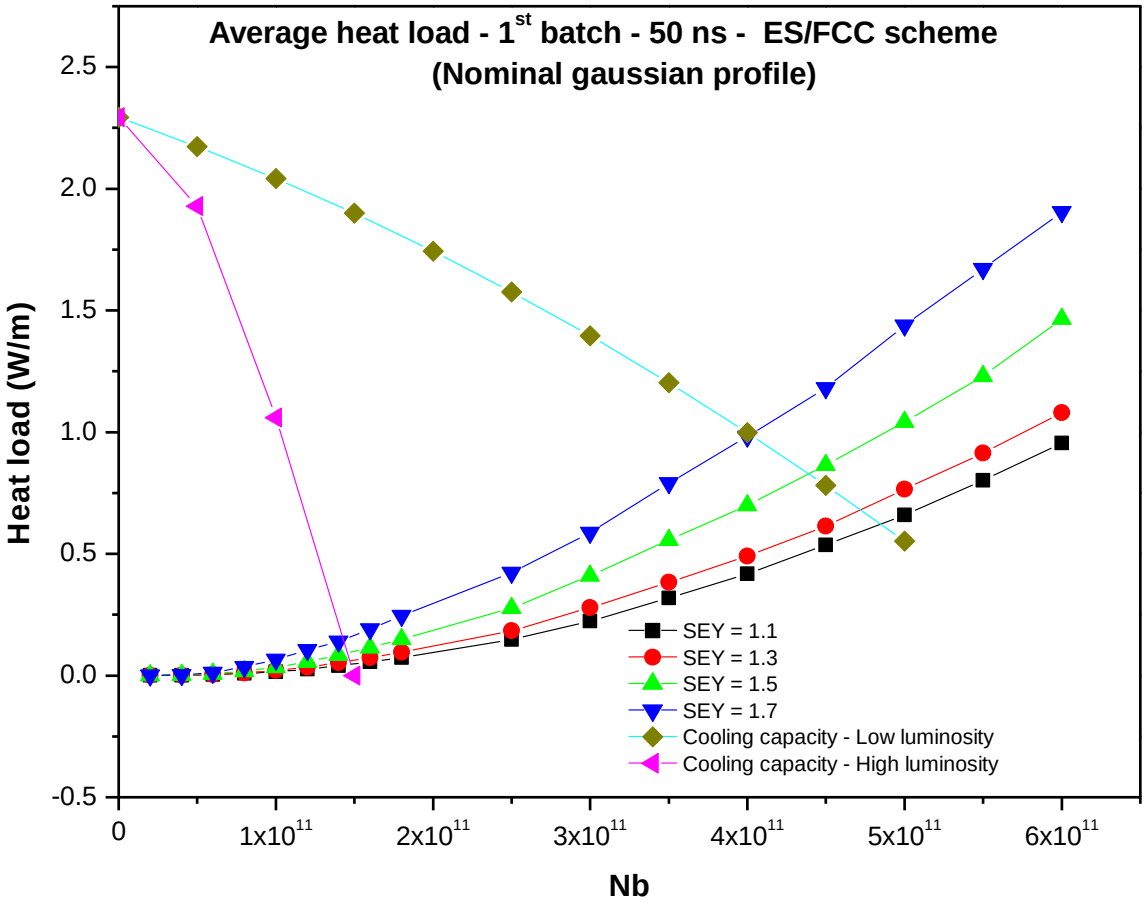

Figure 4.5 Average heat load for the simulation set C, 1st batch.

In Figure 4.6, we present the results for the second batch of the simulation set C.

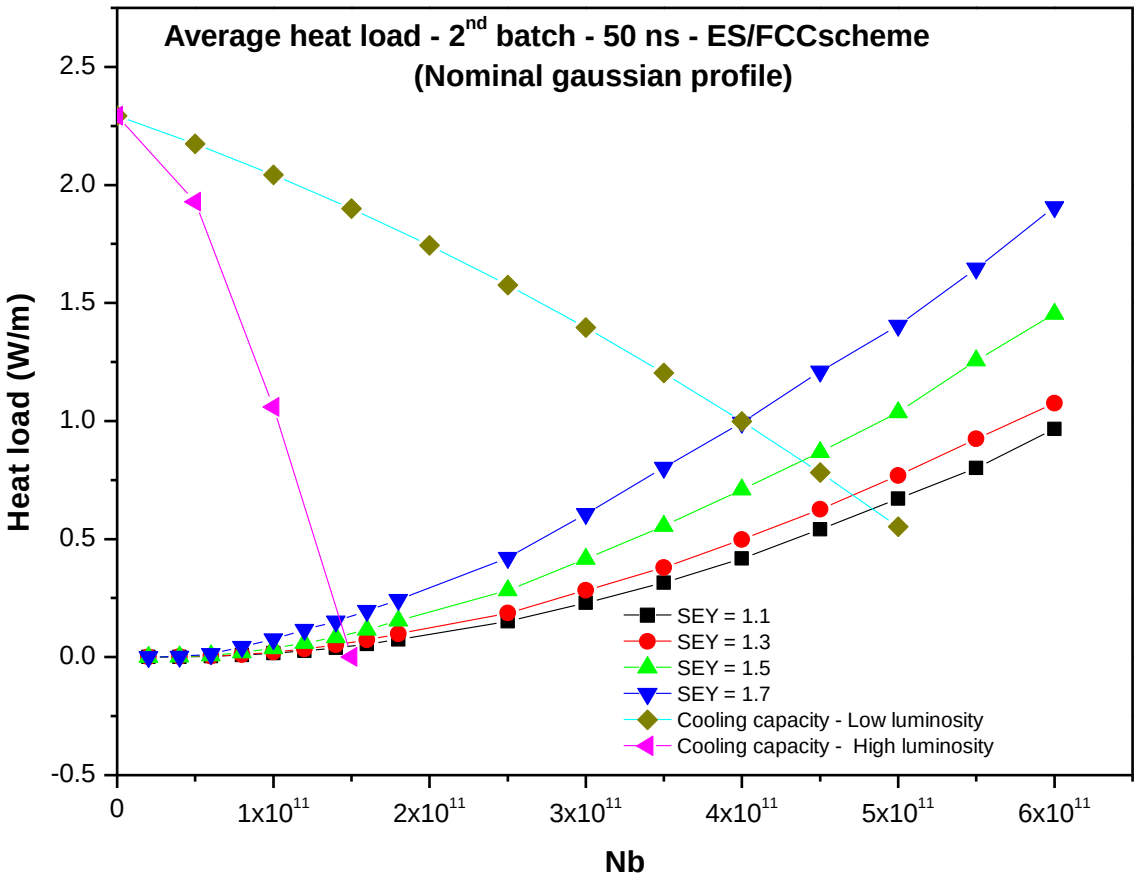

Figure 4.6 Average heat load for the simulation set C, 1st batch.

4.2.2 LPA Scheme

The results of the first batch of set D are shown in Figure 4.7. This scheme differs from prior ones because it has a flat bunch profile instead of the Gaussian bunch profile like the other ones. Like the previous case, this set shows, under certain parameters, higher heat load that exceeds the cooling capacity. In Figure 4.8 we can see the results for the second batch of the simulation set D.

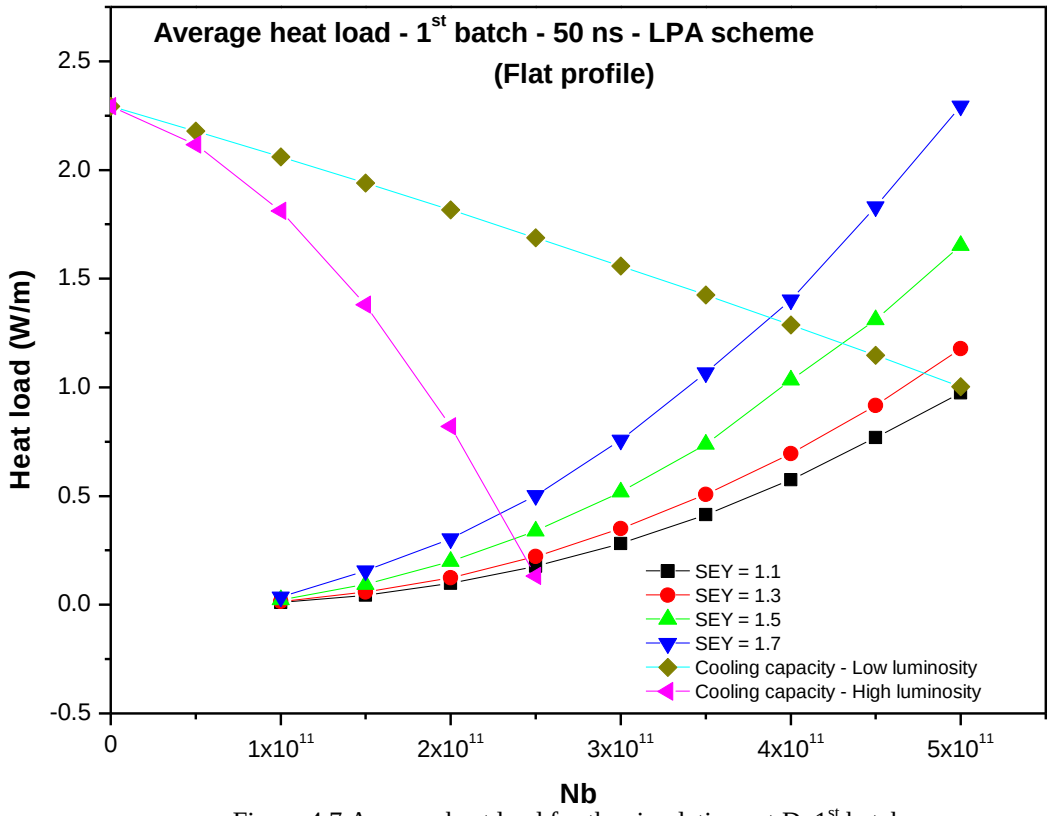

Figure 4.7 Average heat load for the simulation set D, 1st batch.

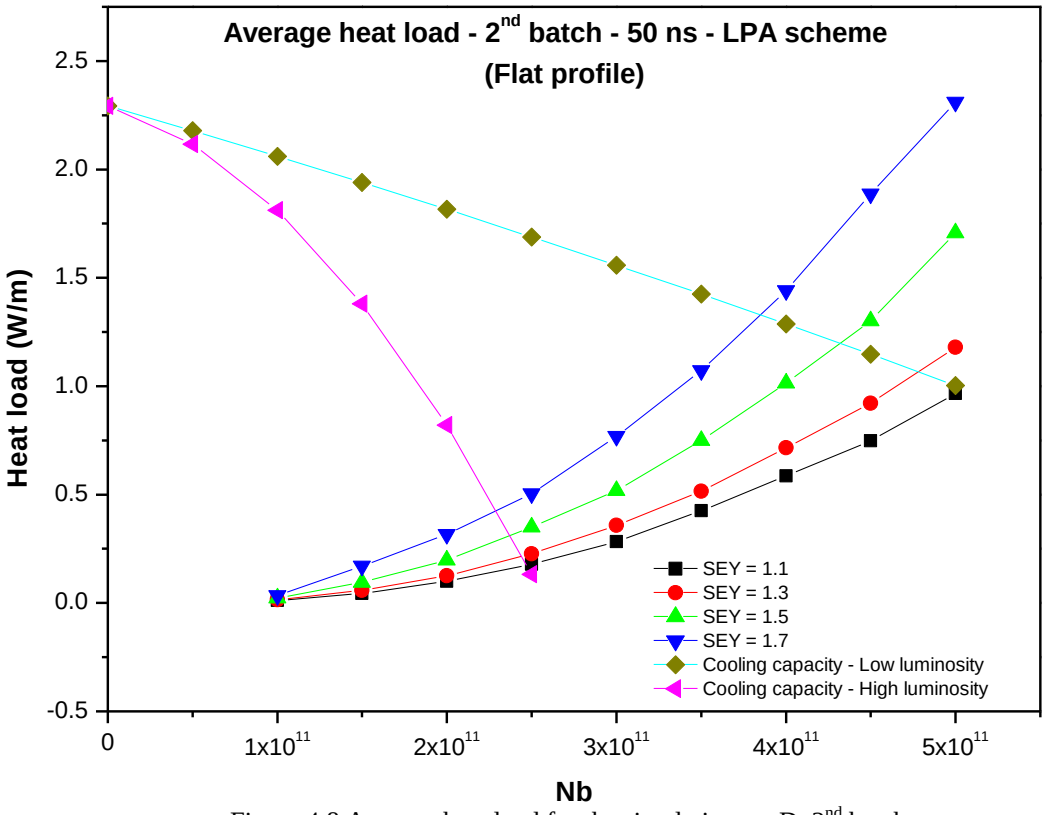

Figure 4.8 Average heat load for the simulation set D, 2nd batch.

4.2.3 Compatibility Scheme with the LHCb Experiment

Below are the graphs of the average heat load for simulation sets E and F. Because there is no significant difference between the first and the second batch, the graphs corresponding to latter will be omitted. In Figure 4.9 we compare the average heat load between the satellite scenario and the nominal scenario without satellite. It can be seen as the heat load is higher for the case with satellites. But the difference is not significant and is still within the acceptable limits of cooling capacity.

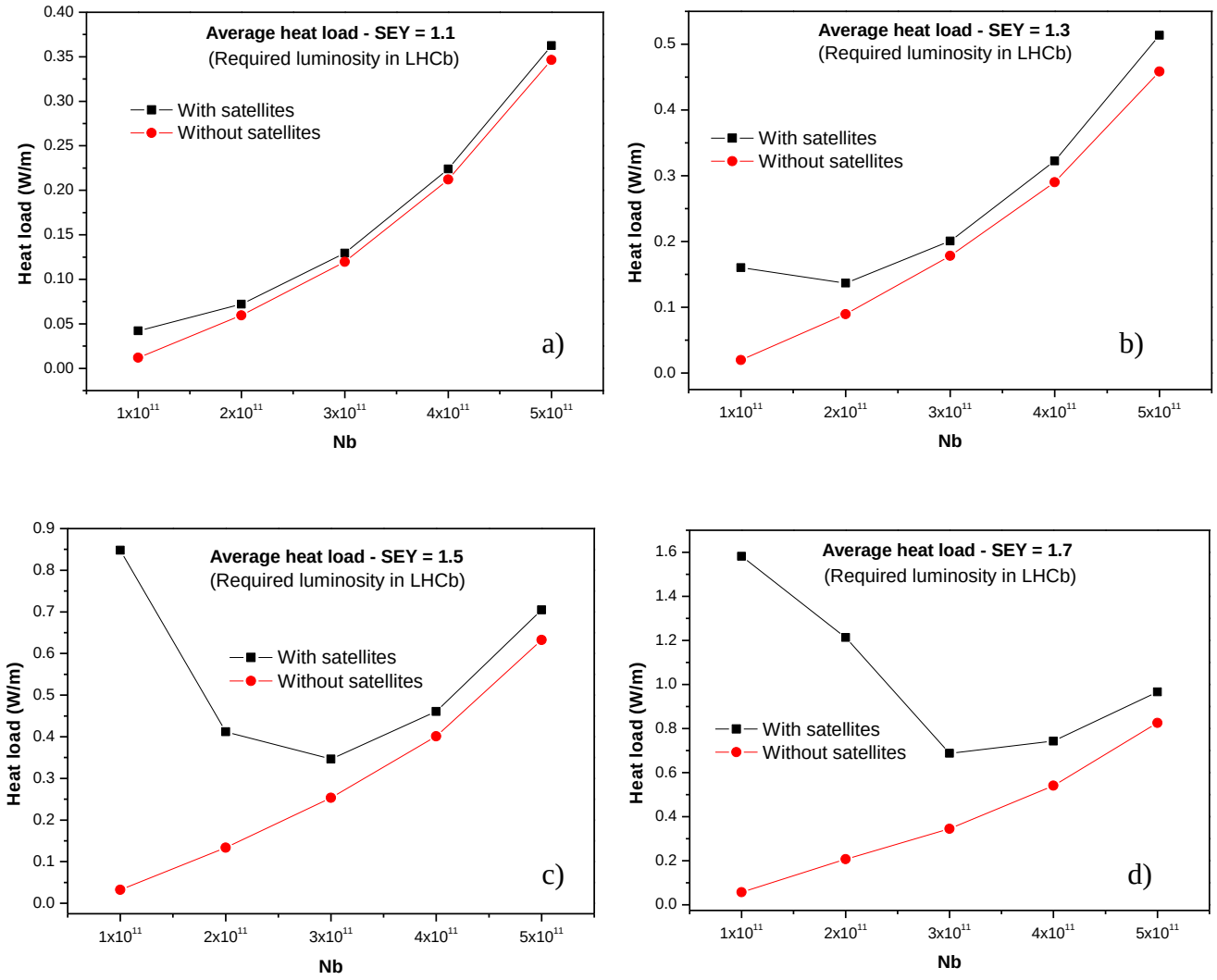

Figure 5.9 Comparison of average heat load for satellite bunches (black line) and the nominal scenario without satellite (red line) for a SEY equal to a) 1.1, b) 1.3, c) 1.5 and d) 1.7.

4.3 Results of Simulations for the Scanning of Bunch Spacing

Below we present the results of the scanning of bunch spacing for two types of bunch profiles: Gaussian and Flat. In Figure 4.10 we present the results for a SEY = 1.1 and both types of bunch profile. As can be seen from the figure the heat load is slightly higher for the Gaussian bunch profile.

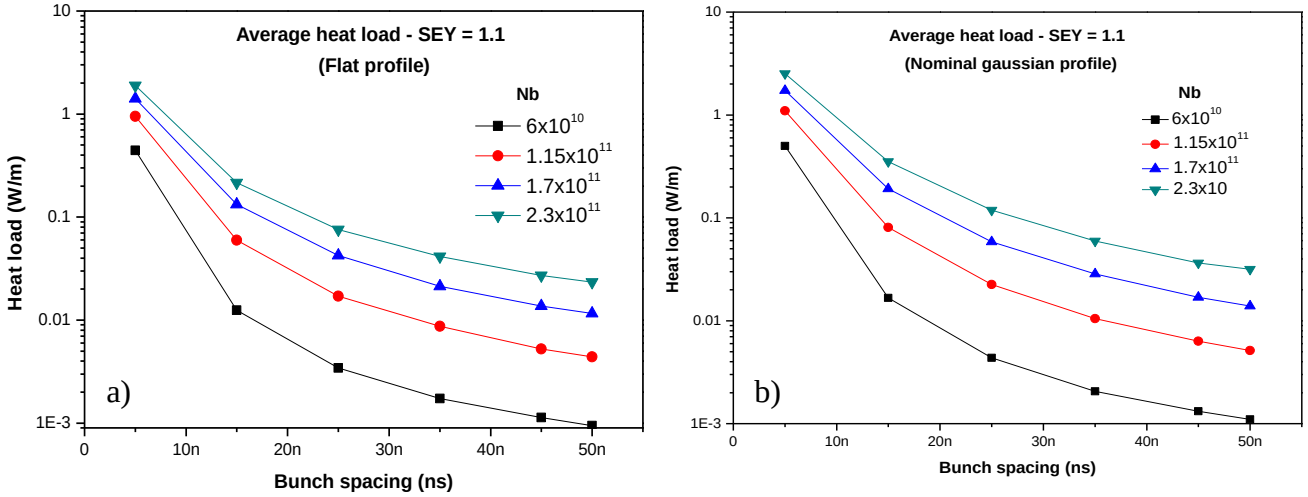

Figure 4.10 Average heat load in function of the bunch spacing and a SEY = 1.1 for a) flat bunch profile and b) nominal Gaussian profile.

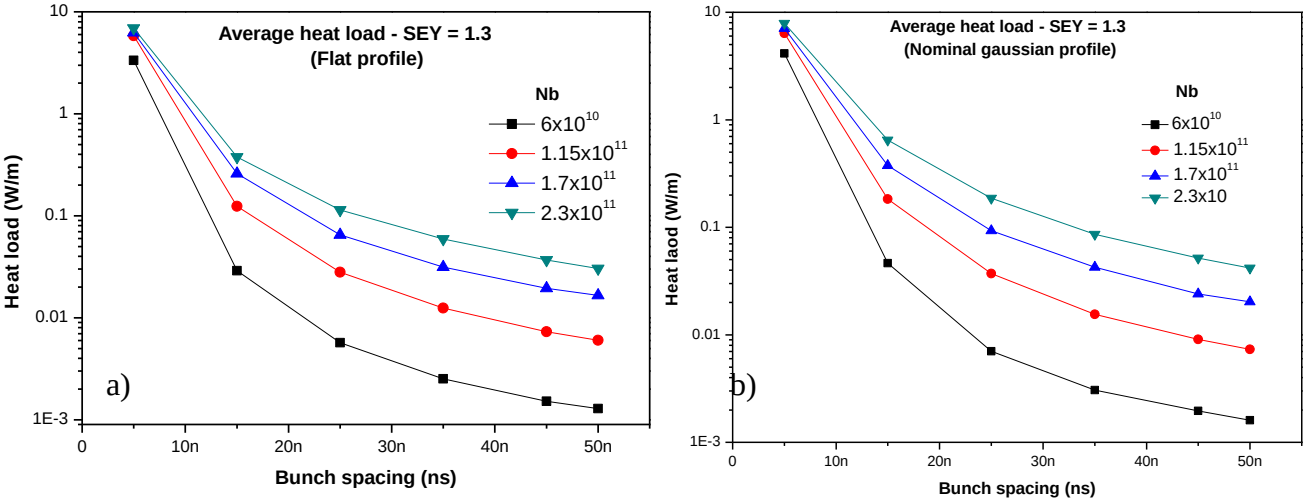

Figure 4.11 Average heat load in function of the bunch spacing and a SEY = 1.3 for a) flat bunch profile and b) nominal Gaussian profile.

For the next SEY considered in the study, we see in Figure 4.11 as the heat load starts to be higher for the nominal Gaussian bunch profile. Figure 4.12 shows the average heat load for a SEY = 1.5, the heat load is less than for the Gaussian profile.

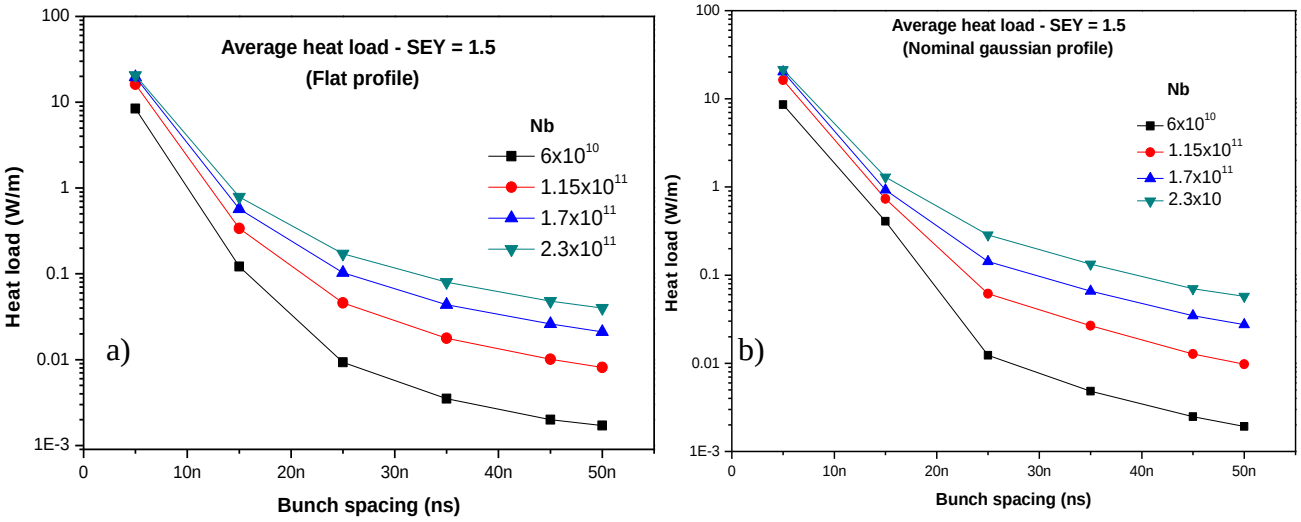

Figure 4.12 Average heat load in function of the bunch spacing and a SEY = 1.5 for a) flat bunch profile and b) nominal Gaussian profile.

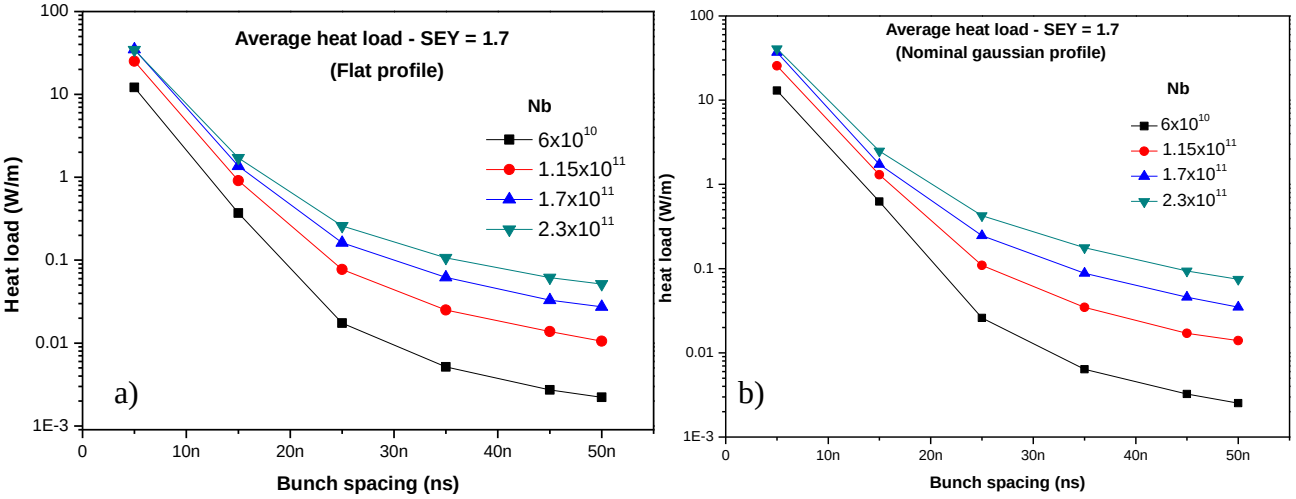

Figure 5.13 Average heat load in function of the bunch spacing and a SEY = 1.7 for a) flat bunch profile and b) nominal Gaussian profile.

Finally, in Figure 4.13 shows the results for a SEY = 1.7 where again be seen as the heat load is higher for the nominal Gaussian bunch profile than for the flat one.

Conclusions

- There is no appreciable difference between the heat load of the first of the first and second batch.
- In the case of 25 ns bunch spacing we conclude that:
  - For a SEY < 1.3, the nominal LHC scheme produces a heat load acceptable.
  - For a SEY < 1.5, a maximum $N_b = 9 \times 10^{10}$ is acceptable.
- For the 50 ns bunch spacing the nominal LHC scheme produces an acceptable heat load until $N_b = 2 \times 10^{11}$.
- Regarding the proposed high-luminosity schemes of the LHC, the heat load is acceptable to:
  - ES/FCC until $N_b = 4.5 \times 10^{11}$
  - LPA, until $N_b = 5.5 \times 10^{11}$
- Regarding the compatibility scheme with the LHCb experiment we have:
  - For a SEY = 1.1 the heat load for the satellite scenario and the nominal scenario without them is almost the same.
  - For a SEY > 1.1 the satellite scenario has a higher heat load than the nominal scheme, however decreases to a minimum value and the difference between the two schemes is less and acceptable.
- Regarding the scanning of bunch spacing was found that to bigger bunch spacing the heat load is lower. Regarding the bunch profiles, we have:
  - For both, the bunch spacing of 50 ns presents the lowest heat load.
  - The nominal Gaussian bunch profile presents a higher heat load than the flat bunch profile.
- Regarding to the bunch length, we conclude that to bigger length the heat load is lower.

Future work

- Perform simulations of experiments in the SPS.
- Study the pressure increase due to the electron cloud in the SPS.
- Compare real data from the electron cloud in the LHC with the simulations.

References

Arduini G., Baglin V., Benedetto E., Cimino R., Collier P., Collins I., Cornelis K., Henrist B., Hilleret N., Jenninger B. (2003). *Present Understanding of Electron Cloud Effects in the Large Hadron Collider*. LHC Project Report 645, Geneva, Switzerland.

Baglin V., Collins R., Grobner O. (1998). "Photoelectron yield and photon reflectivity from candidate LHC vacuum chamber materials with implications to the vacuum chamber design. In proc. 6th European Particle Accelerator Conference (EPAC 98), 2169-2771, Stockholm, Sweden.

Benvenuti C., Chiggiato P., Costa Pinto P., Escudeiro A., Hedly T., Mongelluzzo A., Ruzinov V., Wevers I. (2001). *Vacuum properties of TiZrV non-evaporable getter films.* Vacuum (60), 57-65.

Bhat C. (2009). *Flat bunch creation and acceleration: a possible path for the LHC luminosity upgrade.* In proc. of the conference: FERMILAB-CONF-09-243-AD-APC, 9.

Boussard D., Linnecar T. (1999) *The LHC Superconducting RF System.* LHC Project Report 316.

Caspers F., Rumolo G., Scandale W., Zimmermann F. (2009). *Beam-Induced Multipactoring and Electron-Cloud Effects in Particle Accelerators*. CERN-BE-2009-005.

Cimino R., Baglin V., Collins I.R, Giglia A., Mahne N., Nannarone S., Pasquali L., Pedio M. (2003). *Photon Reflectivity Distributions from the LHC Beam Screen and their Implications on the Arc Beam Vacuum System* LHC Project Report 668.

CERN Press Office (2008). *"First beam in the LHC - accelerating science*". September 10, 2008. http://press.web.cern.ch/press/PressReleases/Releases2008/PR08.08E.html. Web site visited on 2009-07-30.

Chao A. W., Tigner M. (1998). *Handbook of Accelerator Physics and Engineering.* World Scientific Publishing Co. Pte. Ltd., Singapur.

Diaczenko N., Jaisle A., McIntyre P., Pogue N. (2005). *Killing the Electron Cloud Effect in the LHC Arcs.* In procc. 21st IEEE Particle Accelerator Conference, Horak C. (Editor), 2971-2974, Knoxville, USA.

Furman M. y Lambertson G. (1997) *The Electron-Cloud Instability in the Arcs of the PEP-II Positron Ring.* In proc. Internal Workshop on Multibunch Instabilitied in Future Electron and Positron Accelerators, Tsukuba, Japón.

Gupta R., Jain A., Wanderer P., and Willen E. (1998). "*Magnetic design of dipoles for LHC insertion regions,*" in Proc. 6th European Particle Accelerator Conf., Stockholm, Sweden, June 22–26, pp. 1993–1995.

Jimenez J., Arduini G., Collier P., Ferioli G., Henrist B., Hilleret N., Jensen L., Weiss K., Zimmermann F. (2002) *Electron cloud with LHC-type beams in the SPS: A review of three years of measurements.* In proc. Mini-Workshop on electron Cloud Simulations for Proton and Positron Beams (ECLOUD'02), Geneve, Switzerland.

Kirby R., King F. (2000). *Secondary Electron Emission from Accelerator Materials.* In proc. 8th ICFA Beam Dynamics Mini Workshop on "Two-Stream Instabilities".

Koutchouk J.P, Zimmermann F. (2009). *LHC Upgrade Scenarios.* CERN sLHC Project Report.

Rossi L. (2004) Superconducting Magnets for the LHC main Lattice, IEEE Trans. Appl. Supercond.: 14, number 2, pp.153-158.

Ruggiero F., Zimmermann F. *Possible scenarios for an LHC upgrade.* Proceedings 1st CARE-HHH-APD Workshop on Beam Dynamics in Future Hadron Colliders and Rapidly Cycling High-Intensity Synchrotrons, CERN, Geneva, Switzerland, 8 - 11 Nov 2004, pp.1-13.

Scandale W., Zimmermann F. *Scenarios for the LHC Upgrade.* Proceedings of the CARE-HHH-APD Workshop on Interaction Regions for the LHC Upgrade, DAFNE, and SuperB, Frascati, Italy, 6 - 9 Nov 2007, pp.10-18.

Schmidt R. (2003). *The LHC accelerator and its challenges*. Proceedings of the Fifty Seventh Scottish Universities Summer School in Physics, Krämer M. and Soler F.J.P. (Editors), 217-249, St. Andrews, England.

Schulte D., Zimmermann F. (2007). *Electron cloud build-up simulations using Ecloud.* In proc. 31st Advanced ICFA Beam Dynamics Workshop on Electron-Cloud Effects, Napa, CA, USA, 19 - 23 Apr 2004, 143-152.

Vance E. (2006). *Battling the Clouds*. Simmetry Magazine (3), 20-23.

Weisstein E. *Bulirsch-Stoer Algorithm.* MathWorld -A Wolfram Web Resource. http://mathworld.wolfram.com/Bulirsch-StoerAlgorithm.html. Visited on August 7th, 2009.

Wilson E. (2001). *An Introduction to Particle Accelerators*. Oxford University Press.

Zimmermann F. (1997). *A Simulation Study of Electron-Cloud Instability and Beam-Induced Multipacting in the LHC*. LHC Project Report 95, Geneva, Switzerland.

Zimmermann F. y Benedetto E. (2004). *Electron-Cloud Effects in the LHC.* ICFA Newsletter No. 32